

PoSafeNet: Safe Learning with Poset-Structured Neural Nets

Kiwan Wong¹ Wei Xiao²¹ Daniela Rus¹

Abstract

Safe learning is essential for deploying learning-based controllers in safety-critical robotic systems, yet existing approaches often enforce multiple safety constraints uniformly or via fixed priority orders, leading to infeasibility and brittle behavior. In practice, safety requirements are heterogeneous and admit only partial priority relations, where some constraints are comparable while others are inherently incomparable. We formalize this setting as *poset-structured safety*, modeling safety constraints as a partially ordered set and treating safety composition as a structural property of the policy class. Building on this formulation, we propose PoSafeNet, a differentiable neural safety layer that enforces safety via sequential closed-form projection under poset-consistent constraint orderings, enabling adaptive selection or mixing of valid safety executions while preserving priority semantics by construction. Experiments on multi-obstacle navigation, constrained robot manipulation, and vision-based autonomous driving demonstrate improved feasibility, robustness, and scalability over unstructured and differentiable quadratic program-based safety layers.

1. Introduction

Modern robot learning systems increasingly rely on large-scale training and highly expressive function approximators to solve complex tasks such as locomotion (Bommasani, 2021), manipulation (Singh et al., 2022), and autonomous driving (Wang et al., 2024). Despite strong empirical performance, these models typically lack formal safety guarantees, which limits their deployment in safety-critical domains. To address this gap, recent work has integrated formal safety certificates - most notably Control Barrier Function (CBF) (Xiao et al., 2023; 2025) - into learning-based controllers to guarantee safety through forward invariance of a prescribed

safe set.

However, most existing safe learning approaches implicitly assume that multiple safety constraints can be enforced *symmetrically and simultaneously*, typically through a single optimization-based safety layer such as a Differentiable Quadratic Program (dQP) (Amos and Kolter, 2017) or Differentiable Model Predictive Control (dMPC) (Amos et al., 2018). This assumption imposes a restrictive and often unnatural *representation* of safety: it forces the policy to resolve priority conflicts implicitly through optimizations (Choi et al., 2025; Escande et al., 2014) that may lead to infeasibility, rather than explicitly through structure. In realistic robotic systems, safety constraints are heterogeneous (Modugno et al., 2016; Sentis and Khatib, 2005), arising from distinct failure modes, physical limitations, and sensing modalities. Treating such constraints uniformly may lead to inefficiency, infeasibility, excessive conservativeness, or unstable learning behavior under noise and model mismatch.

A key observation motivating this work is that *safety is inherently compositional*. Different safety requirements encode distinct notions of “what must not happen” and are rarely mutually interchangeable. For example, in autonomous driving, reacting to the left and right lane boundaries corresponds to distinct safety primitives that may be individually valid yet structurally incomparable. Crucially, neither enforcing all constraints symmetrically nor imposing an arbitrary total ordering provides an appropriate *inductive bias* for composing such heterogeneous safety requirements.

In many practical settings, safety constraints admit only a partial order, where some priorities are well defined while others are inherently incomparable. This raises a fundamental learning question:

How can we compose multiple safety-critical policies in a scalable and adaptive manner when the underlying safety constraints admit only a partial order, rather than a single global priority?

We argue that a central limitation of existing approaches lies not in the availability of safety certificates themselves, but in the absence of a structural inductive bias governing how such constraints should be composed. A partial order

¹MIT CSAIL, Cambridge, MA, USA ²Worcester Polytechnic Institute, Worcester, MA, USA. Correspondence to: Kiwan Wong, Wei Xiao <kiwan@mit.edu, wxiao3@wpi.edu>.

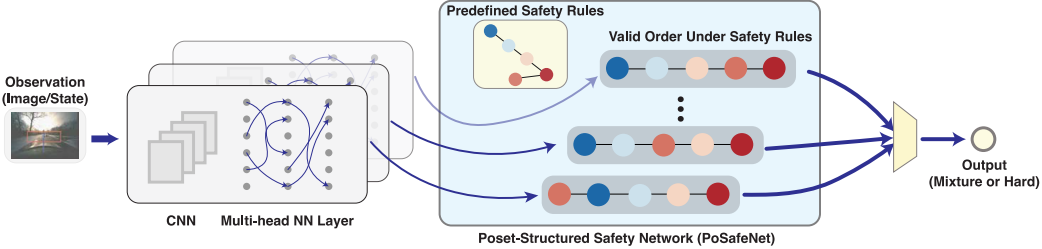


Figure 1. Overview of PoSafeNet. A multi-head neural controller enforces safety through sequential projections under multiple poset-consistent constraint orderings, and adaptively combines the resulting safe executions via a soft mixture or a hard selection.

provides precisely the minimal structure needed: it encodes only the necessary priority relations while leaving incomparable constraints unranked. Accordingly, we model safety composition using a Partially Ordered Set (poset) over safety primitives, treated as *a prior* specified by the designer rather than a learned object.

Building on this perspective, we introduce PoSafeNet (Poset-Structured Safety Network), a learning framework that casts safety composition as a *structured latent decision problem* without solving dQPs. Given a poset over safety constraints, PoSafeNet represents the space of admissible safety executions via its poset-respecting linear extensions. Each execution corresponds to a sequential and analytical safety projection that is provably valid by construction. A multi-head neural architecture parameterizes this discrete set of valid executions, enabling the policy to reason over alternative, priority-consistent safety behaviors.

Crucially, PoSafeNet learns to *select or mix* among these valid executions based on observations, yielding adaptive and context-dependent safety behavior. In effect, the policy operates over a discrete latent space of safety-respecting executions, rather than over unconstrained control actions. This decouples the specification of safety structure from the learning of task behavior, transforming safety enforcement from a constraint satisfaction problem into a structured learning problem with strong guarantees. The PoSafeNet is also more efficient than existing safety neural networks as it admits closed-form projection without solving dQPs.

We make the following **contributions**:

- We introduce *poset-structured safety* as a structural inductive bias for learning-based control, enabling selective and context-dependent resolution of heterogeneous safety priorities.
- We propose PoSafeNet, a neural control framework that enforces *poset-respecting safety* by construction, ensuring that lower-priority constraints are violated only when necessary to enforce higher-priority ones.
- We develop an efficient enforcement of PoSafeNet via closed-form safety projections without solving dQPs.

- We provide formal guarantees that the learned policy satisfies poset-respecting safety under standard assumptions on system dynamics.
- We demonstrate the effectiveness of PoSafeNet on diverse robotic tasks, including 2D obstacle avoidance, safe robot manipulation, and vision-based autonomous driving.

2. Related Work

Scenario-Based and High-Level Safety Frameworks. Scenario-based approaches are widely used for verification and validation of automated driving systems, particularly for identifying safety-critical situations within a given operational design domain (ODD). Zhang et al. (Zhang et al., 2023) provided a comprehensive survey of *critical scenario identification* (CSI) methods for ADS and ADAS, focusing on scenario specification, test generation, and coverage analysis. While these methods are essential for offline evaluation and certification, they do not provide mechanisms for enforcing safety constraints at each control decision during online policy execution.

Beyond scenario analysis, recent work in AI safety emphasizes explicit safety specifications and formal guarantees beyond empirical performance. Dalrymple et al. ("davidad" Dalrymple et al., 2024) propose the *Guaranteed Safe AI* framework, highlighting the roles of specifications, world models, and verification. Related perspectives argue that safety guarantees should be defined in a structured and compositional manner to support formal reasoning and responsibility attribution (Censi et al., 2019). However, these works focus on system-level principles and do not address how multiple safety specifications should be composed and resolved *online* at the level of continuous control actions in learning-based controllers.

In contrast, our work focuses on *online safety enforcement*. We study how multiple safety constraints, potentially related by partial priority relations, can be composed within a differentiable policy and resolved adaptively during execution, enabling end-to-end learning with priority-aware safety guarantees.

Control Barrier Functions and Set Invariance. Set invariance has long been a central concept in control theory for ensuring the safety of dynamical systems (Blanchini, 1999; Rakovic et al., 2005). CBF provide a principled mechanism for enforcing forward invariance of a prescribed safe set by imposing state-dependent constraints on the control input (Ames et al., 2016; Xiao and Belta, 2021). CBFs are closely related to classical barrier functions in optimization (Prajna et al., 2007; Boyd and Vandenberghe, 2004) and are commonly enforced through quadratic programs that can be solved efficiently in real time.

Despite strong theoretical guarantees, CBF-based controllers face feasibility, scalability and robustness challenges when multiple safety constraints must be enforced. Most existing formulations implicitly assume that constraints can be enforced either *symmetrically* as a flat intersection or according to a fixed *total ordering* (Lee et al., 2023). Such assumptions can lead to infeasibility, excessive conservativeness, or brittle behavior when safety requirements are heterogeneous or inherently incomparable.

Safety in Neural Network Controllers. In learning-based control and reinforcement learning, safety is often incorporated through constraint penalties or barrier-based regularization, which typically provide only soft or empirical guarantees (Achiam et al., 2017; Tessler et al., 2018). More recently, differentiable optimization layers have enabled stronger safety guarantees by embedding quadratic programs directly into neural networks (Amos and Kolter, 2017; Pereira et al., 2021; Xiao et al., 2023; 2025). These approaches integrate CBF-based constraints with end-to-end learning, but commonly rely on the *simultaneous enforcement* of multiple constraints or on restricting the number of constraints to maintain feasibility.

As a result, conflicting safety priorities must be resolved implicitly through optimization, without an explicit structural inductive bias governing how such conflicts should be composed. In contrast, our approach models safety priorities explicitly as a *partial order* and enforces constraints through poset-consistent sequential execution. By capturing only the minimal necessary priority relations, we avoid artificial symmetry and brittle total-order assumptions, and enable scalable, priority-aware online safety enforcement within differentiable neural controllers.

3. Problem Formulation

We consider a safe robot learning problem with *poset-structured safety constraints*.

System. Consider a robotic system with state $\mathbf{x} \in \mathbb{R}^n$ and control input $\mathbf{u} \in \mathbb{R}^m$, governed by the control-affine

dynamics

$$\dot{\mathbf{x}} = f(\mathbf{x}) + g(\mathbf{x})\mathbf{u}, \quad (1)$$

where f and g are locally Lipschitz continuous.

Nominal controller. We are given a state-feedback nominal controller $\pi^*(\mathbf{x}) = \mathbf{u}^*$, which provides supervision for learning but does not necessarily enforce safety.

Safety constraints with partial order. Let $\mathcal{S} = \{1, \dots, N\}$ index a set of safety constraints, each represented by a continuously differentiable function $b_j : \mathbb{R}^n \rightarrow \mathbb{R}$, with constraint j satisfied when $b_j(\mathbf{x}) \geq 0$.

The constraints are endowed with a partial order \preceq over \mathcal{S} , where $i \prec j$ indicates that constraint j has strictly higher priority than i . Unlike hierarchical or lexicographic formulations that impose a total order, a partial order allows more complex task specifications with certain constraints to remain incomparable, admitting non-uniform enforcement when necessary to satisfy higher-priority constraints. We define the tuple (\mathcal{S}, \preceq) as a safety poset.

Policy class. We consider a neural network policy

$$\pi(\mathbf{x}, \mathbf{z} \mid \theta) = \mathbf{u}, \quad (2)$$

parameterized by θ , where \mathbf{z} denotes additional observations or contextual inputs. \mathbf{x} may be inferred from \mathbf{z} using a neural network. Safety is enforced implicitly through the structure of the policy class.

Learning objective. The learning objective is to minimize the expected imitation loss

$$\theta^* = \arg \min_{\theta} \mathbb{E}_{\mathbf{x}, \mathbf{z}} [\ell(\pi^*(\mathbf{x}), \pi(\mathbf{x}, \mathbf{z} \mid \theta))], \quad (3)$$

while satisfying the system dynamics and poset-structured safety constraints in \mathcal{S} , with safety enforced by the policy structure rather than explicit constraints in the optimization.

Definition 3.1 (Poset-Respecting Safety). A control policy π satisfies *poset-respecting safety* if there exists a sequential safety enforcement ordering $\sigma = (j_1, \dots, j_N)$ that is a linear extension of the partial order \preceq , such that safety constraints are enforced according to this ordering.

Specifically, a constraint $i \in \mathcal{S}$ may be violated only when enforcing a constraint $j \in \mathcal{S}$ with strictly higher priority, i.e., $i \prec j$. Here, ‘‘before’’ refers to the order of constraint enforcement induced by the policy, rather than physical time.

4. Methodology

In this section, we present PoSafeNet, a learning-based control framework that enforces poset-respecting safety through

structured policy parameterization and differentiable sequential safety projection. Rather than enforcing multiple safety constraints simultaneously - which often leads to infeasible or ill-conditioned optimization problems - PoSafeNet imposes structure on how safety constraints are composed. By treating safety as a structural constraint on the policy class, PoSafeNet enables learnable, priority-aware enforcement of multiple control barrier functions while *preserving feasibility of the safety projection step by construction*.

4.1. Safety Constraints as Halfspace Projections

We first describe how individual safety constraints can be operationalized in the control input space. Consider a safety constraint $b_j(\mathbf{x}) \geq 0$ defined in Section 3. Although safety constraints may be nonlinear in the state space, their enforcement for control-affine systems induces an affine condition on the control input. For systems of the form $\dot{\mathbf{x}} = f(\mathbf{x}) + g(\mathbf{x})\mathbf{u}$, enforcing such a constraint yields

$$A_j(\mathbf{x})\mathbf{u} \geq c_j(\mathbf{x}), \quad (4)$$

where $A_j(\mathbf{x}) \in \mathbb{R}^{1 \times m}$ and $c_j(\mathbf{x}) \in \mathbb{R}$ depend on the system dynamics and the constraint function b_j . This inequality defines a halfspace in the control input space.

$$H_j(\mathbf{x}) := \{\mathbf{u} \in \mathbb{R}^m \mid A_j(\mathbf{x})\mathbf{u} \geq c_j(\mathbf{x})\}. \quad (5)$$

Safety is enforced by projecting a nominal control input \mathbf{u}_{nom} onto the feasible halfspace associated with constraint j . Specifically, we define the projection operator

$$\Pi_j(\mathbf{u}) = \arg \min_{\mathbf{v} \in \mathbb{R}^m} \|\mathbf{v} - \mathbf{u}\|^2 \quad \text{s.t. } A_j(\mathbf{x})\mathbf{v} \geq c_j(\mathbf{x}). \quad (6)$$

We obtain the closed-form solution of the projection operator (6):

$$\Pi_j(\mathbf{u}) = \mathbf{u} + \frac{\text{ReLU}(c_j(\mathbf{x}) - A_j(\mathbf{x})\mathbf{u})}{\|A_j(\mathbf{x})\|^2} A_j(\mathbf{x})^\top. \quad (7)$$

In the above, if the constraint is already satisfied, i.e., $A_j(\mathbf{x})\mathbf{u} \geq c_j(\mathbf{x})$ we have that $\Pi_j(\mathbf{u}) = \mathbf{u}$. The ReLU term enforces the minimal correction required to restore feasibility. This formulation makes explicit that each safety constraint acts as an operator on the control input rather than as a penalty term in the learning objective. Details on constructing (A_j, c_j) from control barrier functions, as well as the conditions under which the closed-form solution applies, are provided in Section A.

Learnable constraint tightness. The affine inequality $A_j(\mathbf{x})\mathbf{u} \geq c_j(\mathbf{x})$ depends on the choice of the class- \mathcal{K} function used in the control barrier condition. For a standard CBF constraint of the form

$$\dot{b}_j(\mathbf{x}, \mathbf{u}) \geq -\kappa_j b_j(\mathbf{x}), \quad (8)$$

the resulting coefficients (A_j, c_j) depend on the scalar gain κ_j . In PoSafeNet, κ_j is treated as a *learnable parameter* optimized jointly with the policy via imitation learning. Although κ_j is fixed across states during execution, learning its value allows the model to learn less conservative policies and adjust the overall tightness of each safety constraint while preserving affine halfspace structure for any $\kappa_j \geq 0$.

4.2. Sequential Safety Projection

While a single safety constraint can be enforced through projection, multiple constraints are composed by applying their projection operators sequentially. Let $\sigma = (j_1, j_2, \dots, j_N)$ denote an ordering of constraint indices in \mathcal{S} . Starting from a nominal control input \mathbf{u}_{nom} , we define

$$\mathbf{u}^{(0)} = \mathbf{u}_{\text{nom}}, \quad \mathbf{u}^{(k)} = \Pi_{j_k}(\mathbf{u}^{(k-1)}), \quad k = 1, \dots, N. \quad (9)$$

where Π_{j_k} is the closed-form projection operator defined in (7). The final control input induced by order σ is $\mathbf{u}_\sigma = \mathbf{u}^{(N)}$. Different orders can yield different control actions even from the same nominal input, motivating the need for a principled structure over admissible constraint orders.

In PoSafeNet, this operator is instantiated per head by applying it to the corresponding nominal policy $\mathbf{u}_{\text{nom}}^{(h)}$ associated with a linear extension $\sigma^{(h)}$.

4.3. Poset-Structured Safety Composition

We adopt the partial order (\mathcal{S}, \preceq) over safety constraints introduced in Section 3. A total order $\sigma = (j_1, \dots, j_N)$ is called a *linear extension* of the poset (\mathcal{S}, \preceq) if for any $i, j \in \mathcal{S}$, $i \prec j$ implies that i appears before j in σ . Each linear extension σ therefore defines a concrete sequential safety enforcement order.

Corollary 4.1 (Poset consistency of linear extensions). *Let (\mathcal{S}, \preceq) be a safety poset. For any linear extension σ of the safety poset (\mathcal{S}, \preceq) , sequential enforcement of constraints as in (9) according to σ satisfies poset-respecting safety in the sense of Definition 3.1.*

Proof. By definition of a linear extension, if $i \prec j$ then i appears before j in σ . Thus, constraint i can only be overridden when enforcing a strictly higher-priority constraint j , which matches the definition of poset-respecting safety. \square

Corollary 4.1 establishes that each individual linear extension corresponds to a valid safety execution, forming the basis for representing multiple admissible safety compositions within PoSafeNet.

Theorem 4.2 (Poset safety under sequential projection and antichain mixing). *Let (\mathcal{S}, \preceq) be a safety poset. Each constraint $i \in \mathcal{S}$ induces a closed convex feasible set*

$H_i(\mathbf{x}) \subset \mathbb{R}^m$ in control space as introduced in (4). Consider a policy that enforces constraints via sequential projection as in (9), according to any linear extension σ of the poset (\mathcal{S}, \preceq) , and combines multiple such executions only through permutations within antichains. Assume that for any pair of incomparable constraints $i \parallel j$, projection onto one constraint does not violate feasibility of the other (see Appendix B for sufficient geometric conditions). Then the resulting policy satisfies poset-respecting safety in the sense of Definition 3.1.

Geometric Intuition. For two incomparable constraints, the sufficient condition requires the projecting of one constraint does not move the control outside the feasible region of the other. Geometrically, the control halfspaces must intersect robustly, avoiding acute corners where projection onto one necessarily violates the other.

In our experiments, the navigation and manipulation tasks are designed to satisfy these sufficient conditions and therefore admit formal guarantees, whereas the vision-based driving task may violate them; in that case, safety guarantees should be interpreted as empirical.

The formal proof and sufficient geometric conditions for Theorem 4.2 are provided in Appendix B.

4.4. PoSafeNet Architecture

PoSafeNet is instantiated as a multi-head neural network. Given state \mathbf{x} and observations \mathbf{z} , the network produces H nominal control inputs $\{\mathbf{u}_{\text{nom}}^{(h)}\}_{h=1}^H$, each associated with a fixed linear extension $\sigma^{(h)}$. Each head applies the corresponding sequential safety projection:

$$\mathbf{u}^{(h)} = \Pi_{\sigma^{(h)}}(\mathbf{u}_{\text{nom}}^{(h)}). \quad (10)$$

All heads operate under a shared poset-structured safety specification and differ in their admissible execution orders, while safety semantics are fixed by a single shared poset.

Head combination and selection. During training, admissible safety executions are combined using a convex mixture with global coefficients:

$$\mathbf{u} = \sum_{h=1}^H \alpha_h \mathbf{u}^{(h)}, \quad \alpha_h \geq 0, \quad \sum_h \alpha_h = 1. \quad (11)$$

Alternatively, a Gumbel-softmax mechanism samples a single head differentiably during training. At inference time, either a single head is selected or a fixed mixture is applied, yielding a deterministic safe control input.

Choice of linear extensions. While the number of linear extensions of a poset can be exponential, PoSafeNet

instantiates a finite set of H heads in practice. We include canonical extensions that respect obvious semantic hierarchies (e.g., collision avoidance or joint limits before task objectives), and sample additional extensions when necessary to cover diverse priority orderings. Empirically, we observe diminishing returns beyond a small H , which we fix across experiments.

4.5. Training and Inference

PoSafeNet is trained via imitation learning on demonstrations $(\mathbf{x}, \mathbf{z}, \mathbf{u}^*) \sim \mathcal{D}$ by minimizing

$$\mathcal{L}(\theta) = \mathbb{E}_{(\mathbf{x}, \mathbf{z}, \mathbf{u}^*) \sim \mathcal{D}} [\ell(\mathbf{u}^*, \mathbf{u}(\mathbf{x}, \mathbf{z}; \theta))]. \quad (12)$$

For each head, gradients propagate through the differentiable projection operators, enabling joint optimization of nominal policy parameters and constraint modulation parameters.

PoSafeNet instantiates a set of nominal control policies, each associated with a fixed linear extension of the safety poset. For a given state, each head produces a nominal control input, which is then mapped to a safe control via sequential projection onto the corresponding constraint-induced halfspaces. During training, head outputs are combined either through convex mixing or differentiable hard selection, while gradients propagate through the projection operators to optimize the nominal policies. The overall construction and inference procedure is summarized in Algorithm 1.

Safety preservation. Learning and stochasticity in PoSafeNet are restricted to selection among structurally valid safety compositions. Each head satisfies poset-respecting safety by construction, as it executes a single linear extension of the safety poset.

Safety remark. Hard head selection is always safe, since it executes one poset-consistent linear extension. Convex mixtures preserve safety only under additional geometric assumptions (Appendix B), namely when all heads lie within a common intersection of halfspaces or when incomparable constraints are mutually non-conflicting. Outside these conditions, convex mixture should be interpreted as an empirical performance heuristic rather than a formal safety guarantee.

As a result, PoSafeNet preserves the specified safety priority semantics by construction, with formal guarantees for hard selection and conditional guarantees for mixture.

5. Experiments

In this section, we evaluate PoSafeNet through a series of experiments designed to answer the following questions:

Algorithm 1 Construction and training of PoSafeNet

Input: $\dot{x} = f(\mathbf{x}) + g(\mathbf{x})\mathbf{u}$; CBF constraints $\{b_i(\mathbf{x}) \geq 0\}_{i \in \mathcal{S}}$ with poset (\mathcal{S}, \preceq) ; linear extensions $\{\sigma^{(h)}\}_{h=1}^H$.

Output: safe control $\mathbf{u}(\mathbf{x}, \mathbf{z})$.

```

1: Initialize nominal policies  $\{\mathbf{u}_{\text{nom}}^{(h)}\}_{h=1}^H$ 
2: Initialize mixture weights  $\alpha$  or Gumbel logits  $\gamma$ 
3: Construct control-feasible halfspaces  $H_i(\mathbf{x})$  as in (4)
    and projection operators  $\Pi_i$  as in (7)
4: for  $h = 1, \dots, H$  do
5:    $\mathbf{u}^{(h)} \leftarrow \mathbf{u}_{\text{nom}}^{(h)}(\mathbf{x}, \mathbf{z})$ 
6:   for  $j \in \sigma^{(h)}$  do
7:      $\mathbf{u}^{(h)} \leftarrow \Pi_j(\mathbf{u}^{(h)}; \mathbf{x})$ 
8:   end for
9: end for
10: Select or mix  $\{\mathbf{u}^{(h)}\}$  using  $\alpha$  or Gumbel-softmax as
    described in Section 4.4, to obtain  $\mathbf{u}(\mathbf{x}, \mathbf{z})$ 

```

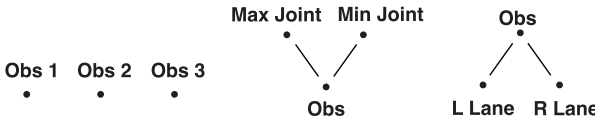
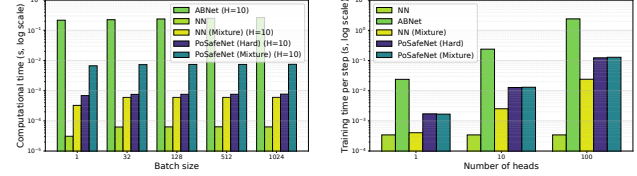


Figure 2. Task-specific safety posets used in the experiments. Left: unicycle navigation with mutually incomparable obstacle constraints. Middle: manipulator task where joint-limit constraints take precedence over obstacle avoidance. Right: vision-based driving where collision avoidance has higher priority than lane keeping.

- How does PoSafeNet compare with unstructured safety layers, including differentiable QP-based methods and prior neural barrier networks, in terms of computational efficiency and training scalability?
- Does enforcing safety through poset-structured sequential projection improve robustness and feasibility compared to simultaneous or slack-based enforcement, especially as the number of safety constraints increases?
- Can PoSafeNet reliably enforce poset-respecting safety in scenarios with conflicting constraints, where not all safety objectives can be satisfied simultaneously?
- How does composing multiple poset-consistent safety policies, through head selection or convex mixture, affect safety, smoothness, and closed-loop performance?

Task-specific safety posets. Figure 2 visualizes the safety posets used in each task. Nodes represent safety constraints and edges indicate strict priority relations. These posets define the admissible safety compositions enforced by PoSafeNet in the following experiments.

Benchmark Models. We compare PoSafeNet against a diverse set of baseline and state-of-the-art methods spanning



(a) Inference (forward-only) time versus batch size with $H = 10$ (log scale).

(b) Training time per step versus number of heads with $B = 128$ (log scale).

Figure 3. Computational efficiency and scalability of PoSafeNet. (a) Inference cost versus batch size. (b) Training time per step versus number of heads. PoSafeNet scales near-linearly in heads and is significantly faster than QP-based safety layers.

end-to-end learning, unstructured safety enforcement, and ensemble-based robustness. (1) **End-to-end neural network (E2E)**, a plain neural network policy trained end-to-end without explicit safety constraints (Levine et al., 2016; Amini et al., 2022); (2) **Unstructured safety layers**, including BarrierNet (Xiao et al., 2023), ABNet (Xiao et al., 2025), and DFBNet (Pereira et al., 2021), which enforce safety constraints without modeling priority, typically by flattening all constraints into a single layer or introducing slack variables that allow violations of higher-priority constraints; and (3) **Structured safety (ours)**, which enforces safety through poset-structured sequential projection, producing control outputs via priority-consistent head selection or convex mixture.

Experimental protocol. Safety (min / mean) reports the minimum and average task-specific barrier value over the rollout. Values are normalized per task and are comparable only within each table, not across tasks. Detailed descriptions of datasets, expert demonstrations, rollout horizons, success criteria, safety margin definitions, and timing measurements are provided in Appendix C. All methods are evaluated under identical experimental settings and training protocols.

5.1. Computation and Training Time

We compare the computational efficiency of the proposed PoSafeNet with ABNet (Xiao et al., 2025), which enforces safety through a differentiable quadratic programming (dQP) layer (Amos and Kolter, 2017), as well as with standard neural network baselines. All timing benchmarks are conducted with three simultaneously active CBF constraints, reflecting the target multi-hazard scenarios considered in this work. While ABNet admits a closed-form projection when enforcing at most two linear constraints, this closed-form solution does not generalize to the three-constraint setting evaluated here. Therefore, for a fair and general comparison under multi-constraint settings, we evaluate ABNet using its dQP-based implementation. The dQP

layer is implemented using `qpth` from OptNet.

Figure 3a reports inference time under varying batch sizes with a fixed number of heads ($H = 10$), while Figure 3b shows training time per optimization step as the number of heads increases with a fixed batch size of 128. PoSafeNet exhibits computational costs comparable to standard neural networks up to a small constant factor, while significantly outperforming ABNet, whose QP-based safety layer incurs substantially higher overhead.

All timing experiments are conducted on a single NVIDIA GPU using PyTorch, with QP layers implemented via `qpth`.

5.2. 2D Robot Multi-Obstacle Avoidance

We consider a planar unicycle navigating toward a fixed goal while avoiding three circular obstacles. All methods are evaluated on 24 held-out test episodes with repeated stochastic rollouts under observation noise (100 trials total).

The three obstacle-avoidance constraints are mutually incomparable and form an antichain, so any total ordering would impose arbitrary priorities. QP-based safety layers cannot directly encode this structure and instead rely on simultaneous enforcement, which often leads to infeasibility, or on slack variables with manually chosen weights. We report results for two representative slack settings. In contrast, PoSafeNet models the antichain by enumerating poset-consistent linear extensions and enforcing safety via sequential projection, without introducing artificial priority.

Table 1 summarizes the results. QP-based methods without slack frequently fail due to infeasibility, while slack-based variants trade feasibility for conservative behavior or degraded safety margins. PoSafeNet achieves feasible rollouts with strictly positive safety margins across all trials, with hard head selection attaining a lower final distance to the goal.

Figure 4 shows representative trajectories. QP-based baselines exhibit conservative detours or safety violations, whereas PoSafeNet produces smooth, goal-directed trajectories that remain close to the reference.

5.3. Safe Robot Manipulation under Joint Constraints

For the manipulator task, we evaluate safety-critical control on a two-link planar manipulator with joint limits and obstacle avoidance. All methods are trained via imitation learning and evaluated on a held-out test set under identical protocols. The objective is to track a reference end-effector trajectory while respecting joint-space safety constraints.

Joint-space constraints, captured by the ϕ safety measure, take precedence over end-effector safety, as violating joint limits is unacceptable even if the end-effector must enter forbidden regions. This induces a non-trivial poset with

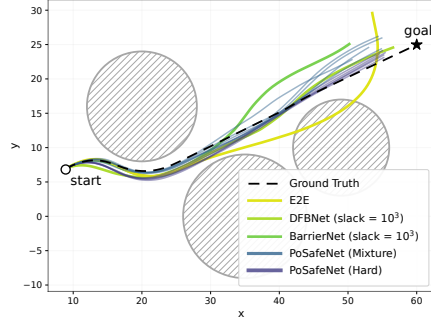


Figure 4. Trajectories for 2D unicycle multi-obstacle avoidance. Representative closed-loop trajectories in a planar navigation task with three circular obstacles in patches. The dashed black curve denotes the reference trajectory. Unstructured baselines exhibit either conservative detours or safety violations. In contrast, PoSafeNet produces smooth, goal-directed trajectories while maintaining safety throughout the rollout.

strict priority relations, in contrast to the antichain structure in the navigation task. QP-based safety layers enforce these heterogeneous constraints either simultaneously or via slack variables, which can lead to numerical instability or residual violations under tight joint limits. In contrast, PoSafeNet directly encodes this precedence relation and enforces safety through sequential projection.

Table 2 summarizes the results. Unstructured baselines frequently exhibit joint-limit violations or instability, even with slack variables. PoSafeNet achieves zero ϕ -violation across all successful episodes while maintaining low tracking error and fast rollout time. Both hard and mixture variants satisfy all joint constraints, with hard selection yielding slightly lower computation cost and mixture yielding lower reference error.

Figure 5 shows representative end-effector trajectories. Unstructured methods exhibit oscillations or violations near joint limits, whereas PoSafeNet closely tracks the reference while respecting all constraints.

5.4. Vision-Based End-to-End Autonomous Driving

We evaluate PoSafeNet on a vision-based autonomous driving task in the VISTA simulator, where policies map raw visual observations directly to control actions. All methods are trained via imitation learning and evaluated on a held-out test set under identical protocols. Safety constraints include collision avoidance and lane keeping, with the objective of driving forward smoothly without crashes.

Collision avoidance takes precedence over lane keeping, allowing lower-priority constraints to be temporarily violated to preserve higher-priority safety. QP-based and unstructured safety layers enforce these constraints either simultaneously or via slack variables, which can lead to brittle

Table 1. Benchmark results on 2D unicycle obstacle avoidance (three circular obstacles). Results are reported over 100 stochastic rollouts (24 test episodes with repeated noise; see Appendix C). *QP Succ.%* denotes the fraction of rollouts where the QP-based safety layer remains feasible. *Safety (min / mean)* reports the minimum and mean obstacle-safety margin over the rollout (negative indicates violation). *MSE* is computed w.r.t. the reference trajectory. *Feasibility* indicates whether a control input is produced at all steps. *Top Safety Guarantee* indicates *Safety* ≥ 0 throughout the rollout. Values below 10^{-11} are treated as zero.

Method	QP Succ.% \uparrow	Safety (min / mean) $\geq 0, \downarrow$	MSE (mean / var) \downarrow	FinalDist _{mean} \downarrow	Rollout Time (avg.) (s) \downarrow	Unc. (u1,u2)	Feasibility	Top Safety Guarantee
E2E (Levine et al., 2016)	100	-81.00 / 3.24	$5.72 \times 10^2 / 1.26 \times 10^7$	26.57	0.028	(4.87, 20.98)	✓	✗
DFB (slack=0) (Pereira et al., 2021)	78	-80.78 / 48.68	$8.50 \times 10^{-2} / 3.46 \times 10^{-2}$	19.43	5.52	(0.251, 0.313)	✗	✗
DFB (slack=10 ³) (Pereira et al., 2021)	100	0.144 / 44.66	$2.47 \times 10^{-2} / 4.05 \times 10^{-4}$	15.40	6.57	(0.146, 0.167)	✓	✓
BarrierNet (slack=0) (Xiao et al., 2023)	44	-43.99 / 16.94	$1.96 \times 10^{-2} / 3.82 \times 10^{-4}$	7.81	7.09	(0.136, 0.113)	✗	✗
BarrierNet (slack=10 ³) (Xiao et al., 2023)	83	$-1.90 \times 10^{-5} / 32.59$	$3.27 \times 10^{-2} / 1.37 \times 10^{-3}$	14.05	7.54	(0.162, 0.198)	✗	✗
ABNet (slack=0) (Xiao et al., 2025)	35	-61.28 / 44.41	$9.45 \times 10^{-2} / 7.04 \times 10^{-2}$	13.14	36.37	(0.102, 0.383)	✗	✗
ABNet (slack=10 ³) [†] (Xiao et al., 2025)	—	—	—	—	—	—	—	—
PoSafeNet (Mixture)	100	1.63 / 37.20	$2.92 \times 10^{-2} / 1.61 \times 10^{-3}$	12.41	1.51	(0.152, 0.185)	✓	✓
PoSafeNet (Hard)	100	0.00 / 31.63	$2.03 \times 10^{-2} / 4.36 \times 10^{-4}$	10.95	0.276	(0.132, 0.132)	✓	✓

[†] ABNet (slack=0) failed to converge during training; metrics are not reported.

Table 2. Benchmark results on the two-link manipulator under joint and obstacle constraints. Results are reported over the held-out test set (see Appendix C). *Safety (min / mean)* reports the minimum and mean obstacle-safety margin (negative indicates violation). ϕ (*mean / max*) quantifies joint-space violation (lower is better). *MSE* is computed w.r.t. the reference end-effector trajectory. *Feasibility* indicates whether a control input is produced at all steps. *Top Safety Guarantee* indicates zero ϕ -violation throughout the rollout. Values below numerical precision are treated as zero.

Method	QP Succ.% \uparrow	Safety (min / mean) $\geq 0, \downarrow$	MSE (mean / var) \downarrow	ϕ (mean / max) \downarrow	FinalDist _{mean} \downarrow	Rollout Time (avg.) (s) \downarrow	Feasibility	Top Safety Guarantee
E2E (Levine et al., 2016)	100	-12.04 / 2.30	$9.64 \times 10^{-3} / 1.06 \times 10^{-4}$	$2.53 \times 10^{-2} / 1.98 \times 10^{-1}$	0.702	0.021	✓	✗
DFBNet (slack=0) (Pereira et al., 2021)	100	-14.99 / -10.74	$4.04 \times 10^{-1} / 3.95 \times 10^{-2}$	$4.05 \times 10^{-2} / 3.26 \times 10^{-1}$	2.53	1.62	✓	✗
DFBNet (slack=10 ³) (Pereira et al., 2021)	100	-14.84 / -8.08	$3.86 \times 10^{-1} / 3.48 \times 10^{-2}$	$4.99 \times 10^{-6} / 4.56 \times 10^{-5}$	2.29	1.71	✓	✗
BarrierNet (slack=0) (Xiao et al., 2023)	100	-9.63 / 2.23	$1.33 \times 10^{-2} / 1.39 \times 10^{-4}$	$3.29 \times 10^{-2} / 2.51 \times 10^{-1}$	0.672	1.59	✓	✗
BarrierNet (slack=10 ³) (Xiao et al., 2023)	100	-4.07 / 2.21	$1.21 \times 10^{-2} / 1.39 \times 10^{-4}$	0.0000 / 0.0000	0.410	1.60	✓	✓
ABNet (slack=0) (Xiao et al., 2025)	76	-14.35 / 43.13	$1.46 \times 10^{16} / 1.60 \times 10^{234}$	0.417 / 0.838	NaN	0.550	✗	✗
ABNet (slack=10 ³) (Xiao et al., 2025)	84	31.03 / 62.05	$4.20 / 1.48 \times 10^2$	0.167 / 0.837	9.48	0.544	✗	✗
PoSafeNet (Mixture)	100	0.199 / 2.44	$9.08 \times 10^{-3} / 1.12 \times 10^{-4}$	0.0000 / 0.0000	0.361	0.173	✓	✓
PoSafeNet (Hard)	100	0.018 / 1.38	$1.04 \times 10^{-2} / 1.27 \times 10^{-4}$	0.0000 / 0.0000	0.527	0.095	✓	✓

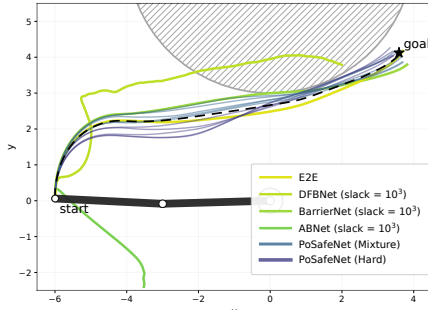


Figure 5. Trajectories for safe robot manipulation under joint-space constraints. Representative end-effector trajectories for a two-link planar manipulator. The dashed black curve denotes the reference trajectory. Unstructured methods exhibit oscillatory or unstable behavior near joint limits. PoSafeNet closely tracks the reference while respecting joint-space safety throughout the rollout.

behavior under visual uncertainty. For comparability, we also report BarrierNet and ABNet without lane constraints.

Table 3 summarizes the results. Unstructured baselines with all constraints imposed either suffer frequent collisions or exhibit unstable behavior near obstacles. Although BarrierNet without lane constraints achieves a lower mean $|e_y|$ in some cases, it lacks an explicit priority structure for resolving heterogeneous safety objectives, resulting in higher variance and less reliable behavior. PoSafeNet trades slight increases in mean deviation for more consistent adherence to safety priorities, achieving a 100% pass rate with zero collisions while maintaining low lane violation and smooth control. The hard and mixture variants attain comparable safety performance, with the mixture producing smoother steering, lower lane violation, and reduced control variance.

Figure 6 shows representative trajectories. Unstructured methods frequently leave the lane or over-correct steering, whereas PoSafeNet maintains lane adherence and collision avoidance throughout the rollout. The mixture variant exhibits improved lane-center adherence, while the hard variant commits to one side of the lane, reflecting selection of a single poset-consistent order. *Additional ablations are provided in Appendix D.*

6. Conclusions, Limitations and Future Work

We propose PoSafeNet, a learning-based control framework that enforces safety through explicit modeling of partial or-

Table 3. Benchmark results on VISTA vision-based autonomous driving. Results are reported over the held-out test set under identical protocols (see Appendix C). *Safety (min / mean)* reports barrier values (negative indicates violation). *Lane viol. (min / mean)* reports lane margin (negative indicates departure). $|e_y|$ (mean / var) quantifies lateral deviation from the lane centerline. *Time-out-of-lane* denotes the fraction of time outside lane boundaries. *Pass%* indicates rollouts completed without collision. *Rot viol.* measures mean rotation rate magnitude. *Uncertainty (u1,u2)* denotes control input standard deviation. Higher is better for Pass and Safety; lower is better for all other metrics.

Method	Pass% \uparrow	Crash% \downarrow	Safety (min / mean) $\geq 0, \downarrow$	Lane viol. (min / mean) \downarrow	$ e_y $ (mean / var) \downarrow	Time-out-of-lane \downarrow	Rot viol. \downarrow	Unc. (u1,u2)
E2E (Amini et al., 2022)	15.0	85.0	-33.63 / -22.39	-1.90 / 0.87	0.396 / 0.330	0.0187	0.07	(0.134, 0.413)
DFBNet (w/ lane constraint) (Pereira et al., 2021)	100.0	0.0	12.36 / 19.07	-2.62 / -1.57	1.509 / 2.745	0.3769	0.52	(0.290, 0.542)
DFBNet (w/o lane constraint) (Pereira et al., 2021)	100.0	0.0	13.11 / 19.73	-2.78 / -1.65	1.514 / 2.871	0.3786	0.61	(0.288, 0.548)
BarrierNet (w/ lane constraint) (Xiao et al., 2023)	0.0	100.0	-44.87 / -31.76	0.07 / 0.09	0.939 / 0.607	0.0000	0.00	(0.038, 0.406)
BarrierNet (w/o lane constraint) (Xiao et al., 2023)	100.0	0.0	-0.17 / 5.82	-4.23 / -1.57	1.364 / 2.522	0.2886	0.73	(0.384, 0.558)
ABNet (w/ lane constraint) (Xiao et al., 2025)	25.0	75.0	-46.16 / -23.60	-0.03 / 0.18	1.174 / 0.433	0.0662	0.00	(0.099, 0.651)
ABNet (w/o lane constraint) (Xiao et al., 2025)	100.0	0.0	5.65 / 8.33	-2.24 / -1.17	1.232 / 2.154	0.3141	0.80	(0.401, 0.423)
PoSafeNet (Mixture)	100.0	0.0	1.23 / 8.21	-0.93 / -0.49	1.028 / 1.278	0.1992	0.14	(0.287, 0.387)
PoSafeNet (Hard)	100.0	0.0	2.73 / 7.12	-0.63 / -0.32	1.404 / 1.599	0.3670	0.80	(0.345, 0.456)

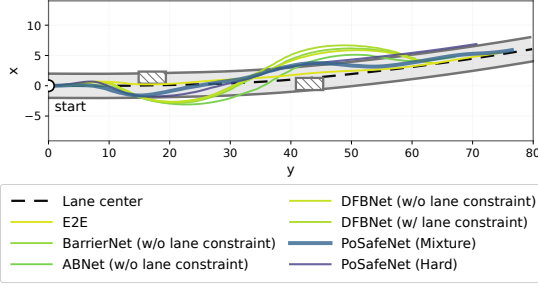


Figure 6. Trajectories for vision-based autonomous driving. Representative closed-loop driving trajectories in the VISTA simulator. Unstructured baselines exhibit unstable behavior near obstacles or lane departures. PoSafeNet maintains collision avoidance and lane adherence throughout the rollout, consistent with the imposed priority of collision avoidance over lane keeping.

ders over safety constraints, enabling systematic relaxation when simultaneous enforcement is infeasible. By treating safety composition as a structural property of the policy class, PoSafeNet enables priority-aware and feasibility-preserving enforcement of multiple control barrier functions via differentiable sequential projection. Across diverse robotic tasks—including multi-obstacle navigation, constrained robot manipulation, and vision-based autonomous driving—we demonstrate that respecting poset-structured safety leads to improved feasibility, robustness, and interpretability compared to unstructured or slack-based safety layers.

Limitations. First, PoSafeNet assumes that a meaningful partial order over safety constraints can be specified or inferred from task semantics; designing such a poset may require domain knowledge. Second, the constraints in PoSafeNet can be designed by prior knowledge in structured environments, but they are not available in unstructured environments. Third, our current formulation focuses on control-affine systems and barrier-based safety certificates, and does not directly address stochastic dynamics or probabilistic safety specifications.

Future Work. Future work will explore automated discovery and learning of safety posets from data, as well as scalable approximations for handling large or dynamic partial orders. Another promising direction is extending PoSafeNet to stochastic and multi-agent settings, where safety priorities may evolve over time or depend on interactions with other agents. Incorporating probabilistic safety guarantees and tighter integration with perception uncertainty also represents an important avenue for deploying poset-respecting safety in real-world robotic systems.

References

Joshua Achiam, David Held, Aviv Tamar, and Pieter Abbeel. Constrained policy optimization. In *International conference on machine learning*, pages 22–31. PMLR, 2017.

Aaron D Ames, Xiangru Xu, Jessy W Grizzle, and Paulo Tabuada. Control barrier function based quadratic programs for safety critical systems. *IEEE Transactions on Automatic Control*, 62(8):3861–3876, 2016.

Alexander Amini, Tsun-Hsuan Wang, Igor Gilitschenski, Wilko Schwarting, Zhijian Liu, Song Han, Sertac Karaman, and Daniela Rus. Vista 2.0: An open, data-driven simulator for multimodal sensing and policy learning for autonomous vehicles. In *2022 International Conference on Robotics and Automation (ICRA)*, pages 2419–2426, 2022. doi: 10.1109/ICRA46639.2022.9812276.

Brandon Amos and J Zico Kolter. Optnet: Differentiable optimization as a layer in neural networks. In *International conference on machine learning*, pages 136–145. PMLR, 2017.

Brandon Amos, Ivan Jimenez, Jacob Sacks, Byron Boots, and J Zico Kolter. Differentiable mpc for end-to-end planning and control. *Advances in neural information processing systems*, 31, 2018.

Franco Blanchini. Set invariance in control. *Automatica*, 35(11):1747–1767, 1999.

Rishi Bommasani. On the opportunities and risks of foundation models. *arXiv preprint arXiv:2108.07258*, 2021.

Stephen Boyd and Lieven Vandenberghe. *Convex optimization*. Cambridge university press, 2004.

Andrea Censi, Konstantin Slutsky, Tichakorn Wongpiromsarn, Dmitry Yershov, Scott Pendleton, James Fu, and Emilio Frazzoli. Liability, ethics, and culture-aware behavior specification using rulebooks. In *2019 international conference on robotics and automation (ICRA)*, pages 8536–8542. IEEE, 2019.

Jason J Choi, Jasmine Jerry Aloor, Jingqi Li, Maria G Mendoza, Hamsa Balakrishnan, and Claire J Tomlin. Resolving conflicting constraints in multi-agent reinforcement learning with layered safety. *arXiv preprint arXiv:2505.02293*, 2025.

David "davidad" Dalrymple, Joar Skalse, Yoshua Bengio, Stuart Russell, Max Tegmark, Sanjit Seshia, Steve Omohundro, Christian Szegedy, Ben Goldhaber, Nora Ammann, Alessandro Abate, Joe Halpern, Clark Barrett, Ding Zhao, Tan Zhi-Xuan, Jeannette Wing, and Joshua Tenenbaum. Towards guaranteed safe ai: A framework for ensuring robust and reliable ai systems, 2024. URL <https://arxiv.org/abs/2405.06624>.

Adrien Escande, Nicolas Mansard, and Pierre-Brice Wieber. Hierarchical quadratic programming: Fast online humanoid-robot motion generation. *The International Journal of Robotics Research*, 33(7):1006–1028, 2014.

Jaemin Lee, Jeeseop Kim, and Aaron D. Ames. Hierarchical relaxation of safety-critical controllers: Mitigating contradictory safety conditions with application to quadruped robots. In *2023 IEEE/RSJ International Conference on Intelligent Robots and Systems (IROS)*, pages 2384–2391, 2023. doi: 10.1109/IROS55552.2023.10342094.

Sergey Levine, Chelsea Finn, Trevor Darrell, and Pieter Abbeel. End-to-end training of deep visuomotor policies. *Journal of Machine Learning Research*, 17(39):1–40, 2016.

Valerio Modugno, Gerard Neumann, Elmar Rueckert, Giuseppe Oriolo, Jan Peters, and Serena Ivaldi. Learning soft task priorities for control of redundant robots. In *2016 IEEE International Conference on Robotics and Automation (ICRA)*, pages 221–226, 2016. doi: 10.1109/ICRA.2016.7487137.

Marcus Pereira, Ziyi Wang, Ioannis Exarchos, and Evangelos Theodorou. Safe optimal control using stochastic barrier functions and deep forward-backward sdes. In *Conference on Robot Learning*, pages 1783–1801. PMLR, 2021.

Stephen Prajna, Ali Jadbabaie, and George J Pappas. A framework for worst-case and stochastic safety verification using barrier certificates. *IEEE Transactions on Automatic Control*, 52(8):1415–1428, 2007.

Sasa V Rakovic, Eric C Kerrigan, Konstantinos I Kouramas, and David Q Mayne. Invariant approximations of the minimal robust positively invariant set. *IEEE Transactions on automatic control*, 50(3):406–410, 2005.

Alessandro Rucco, Giuseppe Notarstefano, and John Hauser. An efficient minimum-time trajectory generation strategy for two-track car vehicles. *IEEE Transactions on Control Systems Technology*, 23(4):1505–1519, 2015.

Luis Sentis and Oussama Khatib. Synthesis of whole-body behaviors through hierarchical control of behavioral primitives. *International Journal of Humanoid Robotics*, 2 (04):505–518, 2005.

Ishika Singh, Valts Blukis, Arsalan Mousavian, Ankit Goyal, Danfei Xu, Jonathan Tremblay, Dieter Fox, Jesse Thomason, and Animesh Garg. Progprompt: Generating situated robot task plans using large language models. *arXiv preprint arXiv:2209.11302*, 2022.

Chen Tessler, Daniel J Mankowitz, and Shie Mannor. Reward constrained policy optimization. *arXiv preprint arXiv:1805.11074*, 2018.

Tsun-Hsuan Wang, Alaa Maalouf, Wei Xiao, Yutong Ban, Alexander Amini, Guy Rosman, Sertac Karaman, and Daniela Rus. Drive anywhere: Generalizable end-to-end autonomous driving with multi-modal foundation models. In *2024 IEEE International Conference on Robotics and Automation (ICRA)*, pages 6687–6694, 2024. doi: 10.1109/ICRA57147.2024.10611590.

Wei Xiao and Calin Belta. High-order control barrier functions. *IEEE Transactions on Automatic Control*, 67(7):3655–3662, 2021.

Wei Xiao, Tsun-Hsuan Wang, Ramin Hasani, Makram Chahine, Alexander Amini, Xiao Li, and Daniela Rus. Barriernet: Differentiable control barrier functions for learning of safe robot control. *IEEE Transactions on Robotics*, 39(3):2289–2307, 2023.

Wei Xiao, Tsun-Hsuan Wang, Chuang Gan, and Daniela Rus. Abnet: Adaptive explicit-barrier net for safe and scalable robot learning. In *Forty-second International Conference on Machine Learning*, 2025.

Xinhai Zhang, Jianbo Tao, Kaige Tan, Martin Törngren, José Manuel Gaspar Sánchez, Muhammad Rusyadi Ramli, Xin Tao, Magnus Gyllenhammar, Franz Wotawa, Naveen Mohan, Mihai Nica, and Hermann Felbinger.

Finding critical scenarios for automated driving systems: A systematic mapping study. *IEEE Transactions on Software Engineering*, 49(3):991–1026, 2023. doi: 10.1109/TSE.2022.3170122.

A. Control Barrier Function

This appendix clarifies how CBF induce affine halfspace constraints in the control input space and provides a closed-form solution to the optimization problem involving a single CBF constraint.

A.1. From CBF Conditions to Control Halfspaces

Consider a control-affine system

$$\dot{\mathbf{x}} = f(\mathbf{x}) + g(\mathbf{x}) \mathbf{u}.$$

Given a continuously differentiable control barrier function $b_j(\mathbf{x})$, the standard CBF condition

$$\dot{b}_j(\mathbf{x}, \mathbf{u}) + \alpha(b_j(\mathbf{x})) \geq 0$$

induces an affine constraint on the control input. Specifically, enforcing the above condition yields

$$A_j(\mathbf{x}) \mathbf{u} \geq c_j(\mathbf{x}), \quad (13)$$

where

$$A_j(\mathbf{x}) := L_g b_j(\mathbf{x}) \in \mathbb{R}^{1 \times m}, \quad c_j(\mathbf{x}) := -L_f b_j(\mathbf{x}) - \alpha(b_j(\mathbf{x})) \in \mathbb{R}.$$

Although safety constraints may be nonlinear in the state space, for control-affine systems they always induce affine halfspace constraints in the control input space.

A.2. Safety Constraints as Halfspace Projections

The affine inequality (13) defines a halfspace in the control input space. Safety can therefore be enforced by projecting a nominal control input \mathbf{u}_{nom} onto the feasible halfspace associated with constraint j .

Specifically, for a candidate control input $\mathbf{u} \in \mathbb{R}^m$, we define the projection operator

$$\Pi_j(\mathbf{u}) = \arg \min_{\mathbf{v} \in \mathbb{R}^m} \frac{1}{2} \|\mathbf{v} - \mathbf{u}\|^2 \quad \text{s.t.} \quad A_j(\mathbf{x}) \mathbf{v} \geq c_j(\mathbf{x}). \quad (14)$$

KKT derivation. For notational simplicity, suppress the state dependence and write $A := A_j(\mathbf{x})$ and $c := c_j(\mathbf{x})$. Consider the projection problem

$$\min_{\mathbf{u} \in \mathbb{R}^m} \frac{1}{2} \|\mathbf{u} - \mathbf{u}_0\|^2 \quad \text{s.t.} \quad A\mathbf{u} \geq c,$$

where \mathbf{u}_0 denotes a given nominal control input.

The Lagrangian is

$$\mathcal{L}(\mathbf{u}, \lambda) = \frac{1}{2} \|\mathbf{u} - \mathbf{u}_0\|^2 + \lambda(c - A\mathbf{u}), \quad \lambda \geq 0.$$

The Karush–Kuhn–Tucker (KKT) conditions are:

- Stationarity:** $(\mathbf{u} - \mathbf{u}_0) - \lambda A^\top = \mathbf{0} \Rightarrow \mathbf{u} = \mathbf{u}_0 + \lambda A^\top$,
- Primal feasibility:** $A\mathbf{u} \geq c$,
- Dual feasibility:** $\lambda \geq 0$,
- Complementary slackness:** $\lambda(c - A\mathbf{u}) = 0$.

Substituting $\mathbf{u} = \mathbf{u}_0 + \lambda A^\top$ into the constraint yields

$$c - A(\mathbf{u}_0 + \lambda A^\top) = (c - A\mathbf{u}_0) - \lambda \|A\|^2,$$

where $\|A\|^2 := A A^\top$ for $A \in \mathbb{R}^{1 \times m}$. If $A\mathbf{u}_0 \geq c$, complementary slackness implies $\lambda = 0$ and the solution is $\mathbf{u}^* = \mathbf{u}_0$. Otherwise, the constraint is active and

$$\lambda^* = \frac{c - A\mathbf{u}_0}{\|A\|^2}.$$

Closed-form solution. Combining both cases, the projection admits the closed-form expression

$$\Pi_j(\mathbf{u}) = \mathbf{u} + \frac{\text{ReLU}(c_j(\mathbf{x}) - A_j(\mathbf{x}) \mathbf{u})}{\|A_j(\mathbf{x})\|^2} A_j(\mathbf{x})^\top. \quad (15)$$

The ReLU term explicitly activates only when the constraint is violated, ensuring that feasible control inputs remain unchanged while infeasible inputs are corrected by an orthogonal projection onto the constraint boundary. This closed-form operator serves as the basic building block for the sequential projection and mixing framework developed in the main text.

B. Geometric Conditions for Safe Sequential Projection and Mixing

This appendix characterizes geometric conditions under which sequential enforcement and convex mixing of multiple CBF constraints preserve feasibility. We also explain why these conditions are frequently satisfied in robotic systems, and how their violation motivates poset-structured safety enforcement.

B.1. CBF Constraints as Control Halfspaces

Consider a control-affine system

$$\dot{\mathbf{x}} = f(\mathbf{x}) + g(\mathbf{x}) \mathbf{u},$$

and a collection of CBF $b_i(\mathbf{x})$. The standard constraint condition

$$\dot{b}_i(\mathbf{x}, \mathbf{u}) + \alpha(b_i(\mathbf{x})) \geq 0$$

induces an affine constraint on the control input of the form

$$A_i(\mathbf{x}) \mathbf{u} \geq c_i(\mathbf{x}), \quad A_i(\mathbf{x}) := L_g b_i(\mathbf{x}) = \nabla b_i(\mathbf{x})^\top g(\mathbf{x}),$$

which defines a halfspace in the control input space. The feasible control set associated with multiple CBF constraints is therefore the intersection of such halfspaces.

B.2. Two Sources of Compatibility Between CBF Constraints

Empirically, sequential projection and convex mixing of CBF constraints often preserve feasibility in robotic systems, though this behavior is not universal. We identify two geometric conditions—acting in different spaces—that explain when such compatibility is expected.

B.2.1. CONDITION C1: ALIGNED REPULSIVE DIRECTIONS IN CONFIGURATION SPACE

Each CBF encodes a repulsive constraint with respect to a hazard in the configuration space \mathbf{q} . For common geometric barriers such as obstacle avoidance, collision radii, or lane boundaries, the gradient $\nabla_{\mathbf{q}} b_i(\mathbf{x})$ points in the direction that locally increases the safety margin.

We assume that, at a given configuration,

$$\nabla_{\mathbf{q}} b_i(\mathbf{x})^\top \nabla_{\mathbf{q}} b_j(\mathbf{x}) \geq 0, \quad i \neq j,$$

that is, the repulsive directions associated with different hazards are not opposing. Geometrically, this corresponds to hazards whose avoidance induces compatible motions (e.g., multiple constraints requiring deceleration or steering in the same general direction).

B.2.2. CONDITION C2: CONTROL-CHANNEL ISOTROPY

Let $g_{\mathbf{q}}(\mathbf{x})$ denote the block of $g(\mathbf{x})$ mapping control inputs to configuration dynamics $\dot{\mathbf{q}}$. We assume that locally

$$g_{\mathbf{q}}(\mathbf{x}) g_{\mathbf{q}}(\mathbf{x})^\top = \gamma(\mathbf{x}) I, \quad \gamma(\mathbf{x}) > 0,$$

or more generally that $g_{\mathbf{q}} g_{\mathbf{q}}^\top$ approximately preserves angles in configuration space. This condition holds exactly for single-integrator models and approximately for many fully actuated or feedback-linearized robotic systems.

B.3. Implication for Control-Space Halfspace Normals

Under Conditions C1–C2, the control-space halfspace normals inherit the alignment of the underlying configuration-space repulsive directions.

Lemma B.1 (Compatibility of CBF halfspaces in control space). *Under Conditions C1–C2, the control-space normals satisfy*

$$A_i(\mathbf{x})^\top A_j(\mathbf{x}) \geq 0, \quad \forall i \neq j.$$

Proof. Restricting attention to the configuration component, we have $A_i(\mathbf{x}) = \nabla_{\mathbf{q}} b_i(\mathbf{x})^\top g_{\mathbf{q}}(\mathbf{x})$. Thus, for any $i \neq j$,

$$\begin{aligned} A_i(\mathbf{x})^\top A_j(\mathbf{x}) &= \nabla_{\mathbf{q}} b_i(\mathbf{x})^\top g_{\mathbf{q}}(\mathbf{x}) g_{\mathbf{q}}(\mathbf{x})^\top \nabla_{\mathbf{q}} b_j(\mathbf{x}) \\ &= \gamma(\mathbf{x}) \nabla_{\mathbf{q}} b_i(\mathbf{x})^\top \nabla_{\mathbf{q}} b_j(\mathbf{x}), \end{aligned}$$

where the second equality follows from Condition C2. By Condition C1 and $\gamma(\mathbf{x}) > 0$, the claim follows. \square

Theorem B.2 (Poset safety under sequential projection and antichain mixing). *Let (\mathcal{S}, \preceq) be a safety poset. Each constraint $i \in \mathcal{S}$ induces a (closed) convex feasible set $H_i \subset \mathbb{R}^m$ in control space; in particular, for CBF halfspaces, $H_i = \{\mathbf{u} : A_i^\top \mathbf{u} \geq c_i\}$.*

Enforcement mechanism. *Fix any linear extension (topological order) $\sigma = (j_1, \dots, j_{|\mathcal{S}|})$ of \preceq such that lower-priority elements appear earlier and higher-priority elements appear later: $i \prec j \Rightarrow i$ appears before j in σ . Given a nominal control u_{nom} , define the sequential enforcement iterates*

$$\mathbf{u}^{(0)} := \mathbf{u}_{\text{nom}}, \quad \mathbf{u}^{(t)} := \Pi_{j_t}(\mathbf{u}^{(t-1)}), \quad t = 1, \dots, |\mathcal{S}|,$$

where Π_j denotes Euclidean projection onto H_j . Let the final output be $u_{\text{out}} := \mathbf{u}^{(|\mathcal{S}|)}$.

Antichain mixing. *Consider K heads that share the same relative order on comparable constraints (i.e., each head uses a linear extension of \preceq) and may differ only by permutations within antichains. Let $\mathbf{u}_r^{\text{out}}$ be the output of head r and define the mixed control $\bar{\mathbf{u}} := \sum_{r=1}^K \theta_r \mathbf{u}_r^{\text{out}}$ with $\theta_r \geq 0$, $\sum_r \theta_r = 1$.*

Compatibility assumption (no override among incomparable constraints). *Assume that for any incomparable pair $i \parallel j$ (neither $i \preceq j$ nor $j \preceq i$), projection onto one constraint does not violate the other:*

$$\mathbf{u} \in H_j \Rightarrow \Pi_i(\mathbf{u}) \in H_j, \quad \mathbf{u} \in H_i \Rightarrow \Pi_j(\mathbf{u}) \in H_i. \quad (\text{NI})$$

For halfspaces, a sufficient condition is $A_i^\top A_j \geq 0$ together with $H_i \cap H_j \neq \emptyset$ (cf. Lemma B.1).

Then the following hold.

1. **(Poset-respecting override during enforcement).** *Along the sequential enforcement process, a constraint i can become violated (i.e., satisfied at some step and violated at a later step) only when enforcing a constraint j with strictly higher priority: $i \prec j$. In particular, no incomparable constraint can override another.*
2. **(Mixing preserves poset-respecting safety).** *Assume furthermore that for every constraint $j \in \mathcal{S}$, each head output satisfies $\mathbf{u}_r^{\text{out}} \in H_j$ whenever j is maximal with respect to \preceq (i.e., it has no higher-priority successor). Then the mixed control $\bar{\mathbf{u}}$ also satisfies all maximal constraints, and the mixed policy preserves poset-respecting safety under Definition 3.1 (with the override rule above): any violation of a lower-priority constraint can only be attributed to enforcing some higher-priority constraint, and mixing does not introduce violations among incomparable constraints.*

Proof. (1) Fix any time t and suppose a constraint i is satisfied at step $t-1$ but becomes violated at step t , i.e., $\mathbf{u}^{(t-1)} \in H_i$ and $\mathbf{u}^{(t)} \notin H_i$. By definition $\mathbf{u}^{(t)} = \Pi_{j_t}(\mathbf{u}^{(t-1)})$. If $i \parallel j_t$, then by the non-interference assumption (NI), $\mathbf{u}^{(t-1)} \in H_i$ would imply $\Pi_{j_t}(\mathbf{u}^{(t-1)}) \in H_i$, contradicting $\mathbf{u}^{(t)} \notin H_i$. Hence i is not incomparable with j_t . Since σ is a linear extension and j_t is enforced at step t , the only remaining possibility consistent with “low-to-high” enforcement is that j_t has higher priority than i , i.e., $i \prec j_t$. Thus i can be overridden only by enforcing a higher-priority constraint.

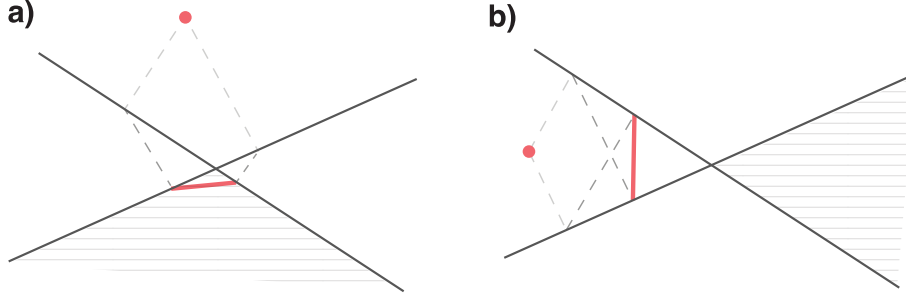


Figure 7. Geometric intuition for compatibility and conflict between CBF constraints. (a) Two CBF halfspaces with non-opposing normals ($A_i^\top A_j \geq 0$). Sequential projection onto one constraint does not violate the other, and the resulting control lies in the intersection of the halfspaces; convex mixing of such controls therefore preserves feasibility. (b) Conflicting CBF constraints with opposing normals ($A_i^\top A_j < 0$), where enforcing one constraint necessarily degrades the other. Such constraints cannot be said to form an antichain and must instead be ordered or prioritized, motivating poset-structured safety enforcement.

(2) Let j be any maximal element of the poset. By assumption, $\mathbf{u}_r^{\text{out}} \in H_j$ for all heads r . Because H_j is convex, it is closed under convex combinations, hence $\bar{\mathbf{u}} = \sum_r \theta_r \mathbf{u}_r^{\text{out}} \in H_j$. Therefore mixing preserves satisfaction of all maximal (highest-priority) constraints. Together with part (1), this implies that (i) violations can only occur by higher-priority overrides, and (ii) incomparable constraints are never made to override each other, which is exactly poset-respecting safety under the stated override rule. \square

B.4. Limitations and the Role of Posets

The above conditions are sufficient but not universal. When multiple hazards induce opposing control corrections—for example, constraints requiring steering in opposite directions or competing accelerations—Condition C1 fails, yielding $A_i^\top A_j < 0$. In this case, enforcing one CBF necessarily degrades another.

Such intrinsically conflicting constraints must therefore be ordered or aggregated, rather than treated as an antichain. The poset structure in our method reflects this geometric compatibility between safety constraints, rather than being an arbitrary design choice.

C. Experimental Details

All quantitative results are reported over $N = 100$ closed-loop evaluation rollouts. For each rollout k , let $b(\mathbf{x}(t)) \geq 0$ denote the task-specific safety barrier function.

Safety (min / mean). We report the minimum and mean safety margin over time and across rollouts, defined as

$$\text{Safety}_{\text{min}} = \min_k \left\{ \min_{t \in [t_0, T]} b(\mathbf{x}(t)) \right\}, \quad \text{Safety}_{\text{mean}} = \mathbb{E}_k \left[\mathbb{E}_{t \in [t_0, T]} \left[b(\mathbf{x}^{(k)}(t)) \right] \right].$$

Negative values indicate violation of the corresponding safety constraint.

Top Safety Guarantee. This metric indicates whether the safety constraint is satisfied at all time steps throughout the rollout. For obstacle avoidance tasks, this corresponds to $\min_t b(\mathbf{x}(t)) > 0$. For joint-space safety, it indicates zero ϕ -violation over the rollout.

Uncertainty. Control uncertainty is quantified as the time-averaged standard deviation of control inputs across rollouts,

$$\text{Unc.}(\mathbf{u}_i) = \mathbb{E}_t \left[\text{std}_k \left(\mathbf{u}_i^{(k)}(t) \right) \right], \quad i \in \{1, 2\}.$$

Feasibility. The *Feasibility* metric indicates whether a valid control input is successfully produced at *every* time step along a closed-loop rollout. A rollout is deemed infeasible if the underlying safety layer fails to return a control input at any time step, for example due to optimization infeasibility, numerical instability, or solver failure. This metric therefore captures the operational reliability of the safety enforcement mechanism, independent of the achieved safety margin.

C.1. 2D Robot Multi-Obstacle Avoidance

To evaluate robustness, we inject zero-mean uniform noise with magnitude 10% of the control input scale during closed-loop execution. For each of the 24 held-out test episodes, we perform multiple stochastic rollouts, resulting in a total of $N = 100$ evaluation runs.

Models. All models use fully connected networks with architecture [5, 128, 32, 32, 2] and ReLU activations. There are some additional layers of differentiable QPs in other models (other than E2E-related models). The model input consists of the system state and the goal.

Training and Dataset. For the 2D robot multi-obstacle avoidance task, the training set consists of 184 trajectories (66,420 state-control pairs), while the held-out test set contains 24 trajectories (8,790 samples), each with approximately 360 time steps. Ground-truth controls are generated by solving higher-order control barrier function (HOCBF)-based quadratic programs that enforce all three obstacle-avoidance constraints simultaneously. All models are trained using the Adam optimizer with an MSE loss and a learning rate of 10^{-3} . Differentiable QP layers are implemented using `qpth` from OptNet. The training time for both PoSafeNet variants (mixture and hard) is approximately one minute for 20 epochs. For multi-head models, ABNet uses 5 heads, while PoSafeNet uses 6 heads.

Robot dynamics and safety constraints. We employ the unicycle model as the robot dynamics:

$$\underbrace{\begin{bmatrix} \dot{x}(t) \\ \dot{y}(t) \\ \dot{\theta}(t) \\ \dot{v}(t) \end{bmatrix}}_{\dot{x}(t)} = \underbrace{\begin{bmatrix} v(t) \cos \theta(t) \\ v(t) \sin \theta(t) \\ 0 \\ 0 \end{bmatrix}}_{f(\mathbf{x})} + \underbrace{\begin{bmatrix} 0 & 0 \\ 0 & 0 \\ 1 & 0 \\ 0 & 1 \end{bmatrix}}_{g(\mathbf{x})} \underbrace{\begin{bmatrix} u_1(t) \\ u_2(t) \end{bmatrix}}_{\mathbf{u}}, \quad (16)$$

where $(x, y) \in \mathbb{R}^2$ denotes the planar position of the robot, $\theta \in \mathbb{R}$ is the heading angle, $v \in \mathbb{R}$ is the linear speed, and u_1 and u_2 are the angular velocity and acceleration controls, respectively.

The obstacle-avoidance safety constraint is defined as

$$b(\mathbf{x}) = (x - x_0)^2 + (y - y_0)^2 - R^2 \geq 0, \quad (17)$$

where $(x_0, y_0) \in \mathbb{R}^2$ denotes the obstacle center and $R > 0$ is its radius.

C.2. Safe Robot Manipulation under Joint Constraints

To evaluate robustness, we inject zero-mean uniform noise with magnitude 10% of the control input scale during closed-loop execution. For each of the 20 held-out test episodes, we perform multiple stochastic rollouts, resulting in a total of $N = 100$ evaluation runs.

Models. All models use fully connected neural networks with architecture [6, 128, 256, 128, 32, 32, 2] and ReLU activation functions. Unstructured safety baselines additionally include differentiable QP layers, whereas the end-to-end (E2E) baseline does not enforce explicit safety constraints.

Training and Dataset. For the safe robot manipulation task, the training set consists of 160 trajectories with approximately 380 time steps each (60,614 state-control pairs). The held-out test set contains 20 trajectories with approximately 370 time steps per trajectory (7,329 samples). Ground-truth controls are generated by solving higher-order control barrier function (HOCBF)-based quadratic programs that enforce only end-effector (obstacle-avoidance) safety, without joint-angle constraints. All models are trained using the Adam optimizer with an MSE loss and a learning rate of 10^{-3} . Differentiable QP layers are implemented using `qpth` from OptNet. The training time for both PoSafeNet variants (mixture and hard) is approximately 24 seconds for 20 epochs. For multi-head models, ABNet uses 5 heads, while PoSafeNet uses 2 heads.

Robot dynamics and safety constraints. We model the two-link planar manipulator using the following control-affine dynamics:

$$\underbrace{\begin{bmatrix} \dot{\theta}_1 \\ \dot{\theta}_2 \\ \dot{\omega}_1 \\ \dot{\omega}_2 \end{bmatrix}}_{\dot{\mathbf{x}}} = \underbrace{\begin{bmatrix} \omega_1 \\ 0 \\ \omega_2 \\ 0 \end{bmatrix}}_{f(\mathbf{x})} + \underbrace{\begin{bmatrix} 0 & 0 \\ 1 & 0 \\ 0 & 0 \\ 0 & 1 \end{bmatrix}}_{g(\mathbf{x})} \underbrace{\begin{bmatrix} u_1 \\ u_2 \end{bmatrix}}_u, \quad (18)$$

where $(\theta_1, \theta_2) \in \mathbb{R}^2$ denote the joint angles, $(\omega_1, \omega_2) \in \mathbb{R}^2$ are the joint angular velocities, and u_1, u_2 are the joint angular acceleration controls.

The end-effector obstacle-avoidance safety constraint is defined as

$$b_{\text{tip}}(\mathbf{x}) = (l_1 \cos \theta_1 + l_2 \cos \theta_2 - x_0)^2 + (l_1 \sin \theta_1 + l_2 \sin \theta_2 - y_0)^2 - R^2 \geq 0, \quad (19)$$

where $(x_0, y_0) \in \mathbb{R}^2$ denotes the obstacle center, $R > 0$ is its radius, and $l_1, l_2 > 0$ are the link lengths. In the current setting, ensuring end-effector safety also guarantees non-collision of the links.

In addition to end-effector safety, we impose joint-angle constraints to prevent excessive bending of the manipulator. We define the relative joint angle

$$\phi = \text{wrap}(\theta_2 - \theta_1) \in [-\pi, \pi), \quad (20)$$

where $\text{wrap}(\cdot)$ maps angles to the principal interval $[-\pi, \pi)$. The corresponding angular velocity is $\dot{\phi} = \omega_2 - \omega_1$.

We enforce joint-angle limits by constraining ϕ to lie within a prescribed interval $[\phi_{\min}, \phi_{\max}]$ using two higher-order control barrier functions:

$$b_{\phi}^{\min}(\mathbf{x}) = \phi - \phi_{\min} \geq 0, \quad (21)$$

$$b_{\phi}^{\max}(\mathbf{x}) = \phi_{\max} - \phi \geq 0. \quad (22)$$

Since ϕ has relative degree two with respect to the control input, with $\ddot{\phi} = u_2 - u_1$, each constraint is enforced via a second-order control barrier function (HOCBF).

These joint-angle constraints are treated as higher-priority safety requirements than the end-effector obstacle-avoidance constraint in the poset, reflecting the fact that joint-limit violations are unacceptable even when obstacle avoidance could otherwise be satisfied.

C.3. Vision-Based End-to-End Autonomous Driving

Models. All methods share the same perception backbone, consisting of a convolutional neural network followed by an LSTM and fully connected control heads. The CNN comprises five convolutional layers with configurations $[3, 24, 5, 2, 2]$, $[24, 36, 5, 2, 2]$, $[36, 48, 3, 2, 1]$, $[48, 64, 3, 1, 1]$, and $[64, 64, 3, 1, 1]$, where each tuple specifies the number of input channels, output channels, kernel size, stride, and padding, respectively. The convolutional features are processed by an LSTM with hidden size 64 to capture temporal dependencies. The control head consists of two fully connected layers of size $[32, 32, 2]$ with ReLU activations, producing the steering rate and acceleration commands.

Dropout with rate 0.3 is applied to both convolutional and fully connected layers during training. Unstructured safety baselines additionally include differentiable QP layers, whereas the end-to-end (E2E) baseline does not incorporate explicit safety constraints. The model input is the front-view RGB image from the ego vehicle with resolution $3 \times 45 \times 155$, and the output is a two-dimensional control vector corresponding to steering rate and longitudinal acceleration.

Training and Dataset. We use a publicly available dataset containing approximately 0.4 million image-control pairs collected in a closed-road sim-to-real driving environment. The dataset is generated using the VISTA simulator (Amini et al., 2022), and includes static and parked vehicles of varying types and appearances as obstacles. Ground-truth control commands are obtained by solving a nonlinear model predictive control (NMPC) problem, which serves as the expert policy for imitation learning. All models are trained using the Adam optimizer with an MSE loss and a learning rate of 10^{-3} . For methods incorporating differentiable safety layers, quadratic programs are solved using `qpth` from OptNet (Amos and Kolter, 2017). Training the PoSafeNet requires approximately 50 minutes for 10 epochs on a single NVIDIA RTX 5090 GPU.

Brief introduction to VISTA. VISTA is a sim-to-real driving simulator that generates diverse driving scenarios from real-world driving data (Amini et al., 2022). We train vision-based policies via guided imitation learning using an expert controller. Data are generated in three steps: (i) VISTA randomly initializes the poses of the ego vehicle and other traffic participants (ado vehicles) consistent with the underlying real driving logs; (ii) a nonlinear model predictive controller (NMPC) is used to compute expert controls and the corresponding state trajectories; and (iii) front-view RGB images are recorded along NMPC rollouts and paired with the expert control commands.

Vehicle dynamics and collision safety constraints. Vehicle dynamics are formulated in a curvilinear coordinate frame defined with respect to a reference trajectory (e.g., the lane centerline) (Rucco et al., 2015). The system state is $\mathbf{x} = [s, d, \mu, v, \delta]^\top$, where $s \in \mathbb{R}$ denotes the progress along the reference trajectory, $d \in \mathbb{R}$ is the lateral offset of the vehicle center, μ is the heading error with respect to the reference trajectory, v is the longitudinal speed, and δ is the steering angle. The control input is $u = [u_1, u_2]^\top$, where u_1 is the steering rate and u_2 is the longitudinal acceleration.

We adopt the curvilinear bicycle model in (Rucco et al., 2015), which can be written in control-affine form as

$$\underbrace{\begin{bmatrix} \dot{s} \\ \dot{d} \\ \dot{\mu} \\ \dot{v} \\ \dot{\delta} \end{bmatrix}}_{\dot{\mathbf{x}}} = \underbrace{\begin{bmatrix} v \cos(\mu + \beta) \\ \frac{1 - dk(s)}{v \sin(\mu + \beta)} \\ v \sin(\mu + \beta) \\ \frac{v}{\ell_r} \sin \beta - \frac{\kappa(s) v \cos(\mu + \beta)}{1 - dk(s)} \\ 0 \\ 0 \end{bmatrix}}_{f(\mathbf{x})} + \underbrace{\begin{bmatrix} 0 & 0 \\ 0 & 0 \\ 0 & 0 \\ 1 & 0 \\ 0 & 1 \end{bmatrix}}_{g(\mathbf{x})} \underbrace{\begin{bmatrix} u_1 \\ u_2 \end{bmatrix}}_u. \quad (23)$$

Collision avoidance is encoded via a control barrier function defined in the curvilinear frame:

$$b_{\text{col}}(\mathbf{x}) = (s - s_0)^2 + (d - d_0)^2 - R^2 \geq 0, \quad (24)$$

where $(s_0, d_0) \in \mathbb{R}^2$ denotes the obstacle location expressed in curvilinear coordinates and $R > 0$ is a safety radius chosen such that satisfying (24) guarantees collision avoidance.

Lane-keeping constraints. Lane keeping is enforced by constraining the lateral offset d of the ego vehicle with respect to the reference trajectory. Specifically, we require the vehicle to remain within a lateral margin $\ell_f > 0$ around the lane centerline:

$$-\ell_f \leq d \leq \ell_f. \quad (25)$$

This is implemented using two higher-order control barrier functions corresponding to the left and right lane boundaries. For the left boundary, we define

$$b_L(\mathbf{x}) = \ell_f - d \geq 0, \quad (26)$$

and for the right boundary,

$$b_R(\mathbf{x}) = d + \ell_f \geq 0. \quad (27)$$

Both constraints are enforced using second-order barrier conditions that account for the vehicle dynamics in the curvilinear coordinate frame, resulting in affine constraints on the control input at each time step.

Closed-loop testing. All methods are evaluated closed-loop in VISTA. At each time step, the policy receives a front-view RGB observation and outputs a control command, which is applied to the simulator. Rollouts terminate when the horizon is reached (or upon collision, when applicable). Unless otherwise stated, we report results over $N = 100$ closed-loop runs.

For each run, the ego vehicle is initialized on the straight segment with $s_0 \sim \mathcal{U}(0, 10)$ m and lateral offset $d \sim \mathcal{U}(-0.5, 0.5)$ m. Two obstacles are placed ahead of the ego vehicle with longitudinal offsets $\Delta s_1 \sim \mathcal{U}(20, 30)$ m and $\Delta s_2 = \Delta s_1 + \mathcal{U}(30, 40)$ m, and lateral offsets sampled uniformly from $\{|d_0| \sim \mathcal{U}(0.1, 1.5)\}$ m with random sign.

Table 4. Ablation benchmark results on VISTA vision-based autonomous driving via PoSafeNet. Results are reported over the held-out test set under identical evaluation protocols (see Appendix C). Safety is quantified by the minimum and mean barrier value over each rollout, where negative values indicate safety violation. Lane keeping performance is measured by the minimum and mean lane margin (lower is better), with negative values indicating lane departure. We additionally report the mean and variance of the absolute lateral deviation $|e_y|$ from the lane centerline to quantify tracking accuracy and lateral stability, as well as the fraction of time the vehicle exceeds lane boundaries (*time-out-of-lane*) as a hard lane violation metric. *Pass%* indicates the percentage of rollouts completed without collision. *Rot viol.* measures the mean rotation rate magnitude, and *Uncertainty* ($u1, u2$) denotes the standard deviation of control inputs over time. Higher is better for Pass and Safety; lower is better for lane violation, $|e_y|$, time-out-of-lane, rotation violation, and uncertainty.

Method	Pass% \uparrow	Crash% \downarrow	Safety (min / mean) > 0	Lane viol. (min / mean) \downarrow	$ e_y $ (mean / var) \downarrow	Time-out-of-lane \downarrow	Rot viol. \downarrow	Unc. ($u1, u2$)
PoSafeNet (Fix Order)	100.0	0.0	0.27 / 3.38	-6.15 / -1.71	1.73 / 3.09	0.3197	0.65	(0.412, 0.641)
PoSafeNet (Wrong Order)	41.0	59.0	-24.42 / -17.70	0.06 / 0.14	0.989 / 0.746	0.0000	0.00	(0.108, 0.742)
PoSafeNet (Mixture)	100.0	0.0	1.23 / 8.21	-0.93 / -0.49	1.028 / 1.278	0.1992	0.14	(0.287, 0.387)
PoSafeNet (Hard)	100.0	0.0	2.73 / 7.12	-0.63 / -0.32	1.404 / 1.599	0.3670	0.80	(0.345, 0.456)

D. Additional Ablations on Order Sensitivity and Control Quality (VISTA)

Effect of Constraint Ordering. To study the sensitivity of sequential safety projection to constraint ordering, we compare four variants that differ only in how lane-keeping and obstacle-avoidance constraints are ordered within the projection pipeline.

In **PoSafeNet (Fix Order)**, obstacle avoidance is enforced as the highest-priority constraint, followed by the left and right lane boundary constraints in a fixed, manually specified order. This design reflects an intuitive safety hierarchy in which collision avoidance strictly dominates lane keeping.

In **PoSafeNet (Wrong Order)**, this hierarchy is intentionally violated by enforcing lane-keeping constraints above obstacle avoidance. This ablation isolates the effect of incorrect cross-priority ordering, where control authority is prematurely consumed by lower-priority constraints, leaving insufficient flexibility to satisfy collision-avoidance objectives.

Although both variants employ the same set of safety constraints, swapping the relative priority between lane keeping and obstacle avoidance leads to qualitatively different outcomes (Table 4). In particular, the wrong-order variant exhibits severe degradation in safety margins and collision performance, demonstrating that incorrect ordering across priority levels can fundamentally compromise safety, even when all constraints are individually feasible.

Interestingly, **PoSafeNet (Fix Order)** remains collision-free with positive minimum barrier values, but incurs substantial lane violations, as evidenced by highly negative lane margins and increased time spent outside lane boundaries. This behavior reflects a structural limitation of rigid, hand-specified ordering: by always enforcing obstacle avoidance first, control authority is exhausted early in the projection pipeline, forcing lower-priority lane constraints to be satisfied only through large lateral deviations.

In contrast, **PoSafeNet (Hard)** learns a global projection strategy via Gumbel-Hard selection over multiple candidate heads, each corresponding to a distinct ordering consistent with the poset structure. By adaptively selecting the ordering that best matches the data distribution, this learned strategy improves safety margins and lane adherence relative to fixed-order baselines.

Finally, **PoSafeNet (Mixture)** softly combines multiple heads to further enhance robustness, yielding smoother control behavior, reduced lateral deviation, lower rotation rates, and less time spent outside lane boundaries, while consistently maintaining collision-free operation.

E. Four-Level Poset Safety Hierarchy for Heatmap Visualization

This appendix describes the four-level safety hierarchy used to generate the heatmap visualizations in the vision-based driving experiments. The purpose is not to introduce new modeling assumptions or additional safety constraints, but to illustrate how refining the priority structure within the same poset-based framework influences closed-loop behavior. In particular, this example highlights the ability of PoSafeNet to incorporate additional low-priority preferences without compromising higher-priority safety requirements.

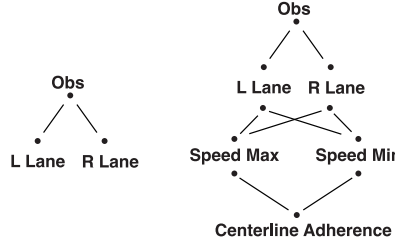


Figure 8. Task-specific safety posets used in the vision-based driving experiments, visualized as Hasse diagrams. Left: a two-level hierarchy where obstacle avoidance has higher priority than left and right lane boundary constraints. Right: a four-level hierarchy that augments the two-level structure with intermediate speed regulation and low-priority centerline adherence, while preserving obstacle avoidance as the highest-priority constraint.

E.1. Poset Structure

Figure 8 compares the task-specific safety posets used in the experiments. The two-level hierarchy enforces only road boundary constraints and obstacle avoidance, whereas the four-level hierarchy further decomposes driving behavior into multiple priority tiers that encode softer preferences.

Formally, we use the partial order symbol \preceq to denote *priority relations* between constraints, where $c_1 \preceq c_2$ indicates that constraint c_1 has lower or equal priority than constraint c_2 . Under this convention, the four-level hierarchy orders constraints from lowest to highest priority as

$$\text{Centerline} \preceq \text{Speed} \preceq \text{Lane} \preceq \text{Obstacle}. \quad (28)$$

Low-priority constraints, such as centerline adherence and speed regulation, are treated as soft behavioral preferences. They are enforced only when doing so does not interfere with higher-priority safety constraints, such as lane boundaries and obstacle avoidance.

E.2. Additional Barrier Definitions

In addition to the lane boundary and obstacle avoidance barriers defined elsewhere, the four-level hierarchy introduces two *additional low-priority* constraints to better capture common driving preferences.

Centerline adherence constraints. Centerline adherence is modeled as a soft preference that encourages the vehicle to remain close to the lane centerline. Let d denote the signed lateral deviation from the lane centerline and $\tau > 0$ a prescribed tolerance. We define two symmetric barrier functions

$$b_{\text{CL},L}(\mathbf{x}) = \tau - d \geq 0, \quad b_{\text{CL},R}(\mathbf{x}) = d + \tau \geq 0. \quad (29)$$

These barriers share the same higher-order control barrier function (HOCBF) structure as the lane boundary constraints, but are enforced at a strictly lower priority level.

Speed regulation constraints. Speed regulation is introduced as a low-priority constraint to discourage overspeeding and excessive braking. Let v denote the vehicle speed and v_{\min}, v_{\max} the desired bounds. We define first-order control barrier functions

$$b_{\max}(v) = v_{\max} - v \geq 0, \quad b_{\min}(v) = v - v_{\min} \geq 0. \quad (30)$$

These constraints yield affine conditions on the longitudinal acceleration and are enforced at a lower priority than lane boundary and obstacle avoidance constraints.

E.3. Interpretation of Heatmaps

The heatmaps illustrate how introducing additional low-priority structure alters the distribution of closed-loop behaviors. Compared to the two-level hierarchy, the four-level hierarchy exhibits reduced lateral deviation and lower overall speed, while preserving collision avoidance and lane safety.

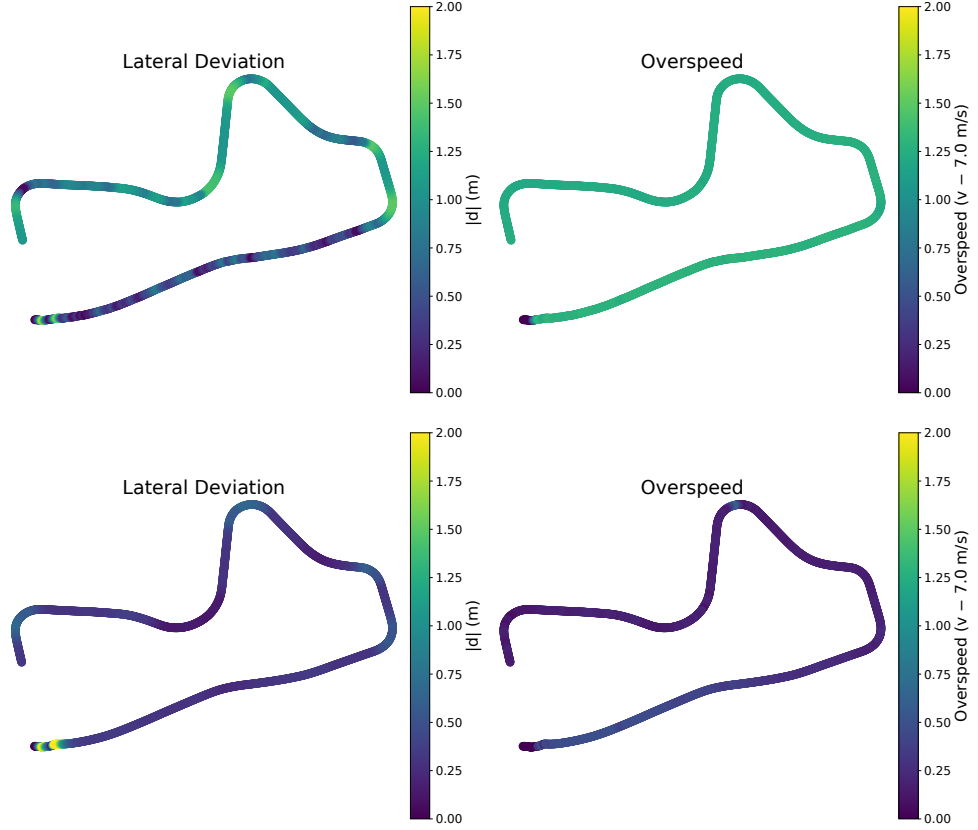


Figure 9. Heatmap visualization of closed-loop driving behavior under different safety hierarchies. Top: two-level poset (lane \preceq obstacle). Bottom: four-level poset (centerline \preceq speed \preceq lane \preceq obstacle). Colors indicate lateral deviation and overspeed along the trajectory.

These results demonstrate that PoSafeNet can absorb additional behavioral preferences by refining the poset hierarchy, shaping closed-loop behavior in a more structured and human-like manner without compromising higher-priority safety constraints. This example therefore serves as a qualitative illustration of the extensibility of the poset-based formulation.

F. Supplementary On Vision Based End-to-End Autonomous Driving

This section provides qualitative visualizations of closed-loop driving behaviors in the VISTA simulator for representative methods. Each snapshot shows the front-view RGB observation received by the policy (left) and a corresponding top-down view of the scene (right), including the ego vehicle, lane centerline, and surrounding obstacles.

These visualizations are intended to complement the quantitative results reported in the main paper by illustrating typical driving behaviors under dynamic obstacle interactions, rather than to serve as a standalone performance comparison.

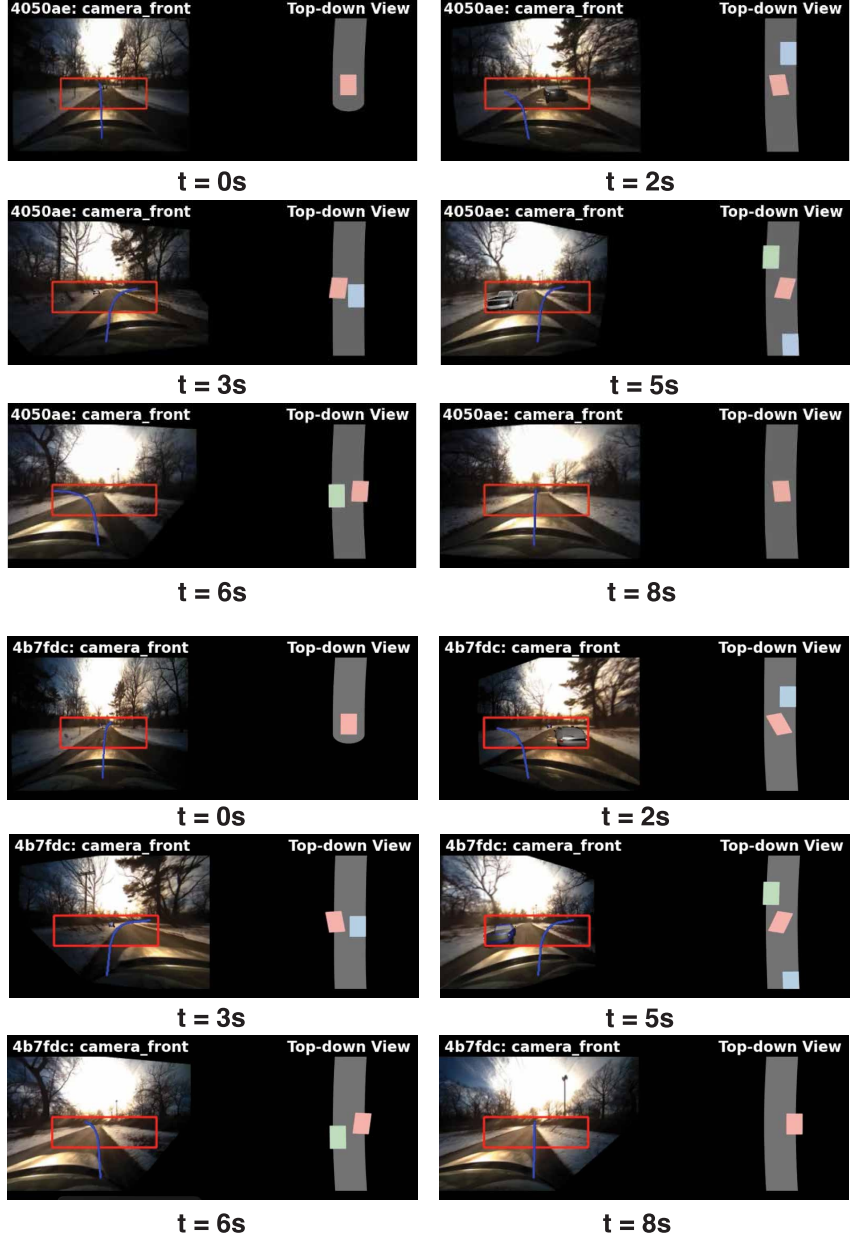


Figure 10. Qualitative visualization of closed-loop driving behaviors in the VISTA simulator. Each snapshot corresponds to a specific time step along the trajectory (timestamps shown above each panel). For each time step, the left image shows the front-view camera observation, while the right image shows the corresponding top-down view. From top to bottom: PoSafeNet (Mixture) and PoSafeNet (Hard).

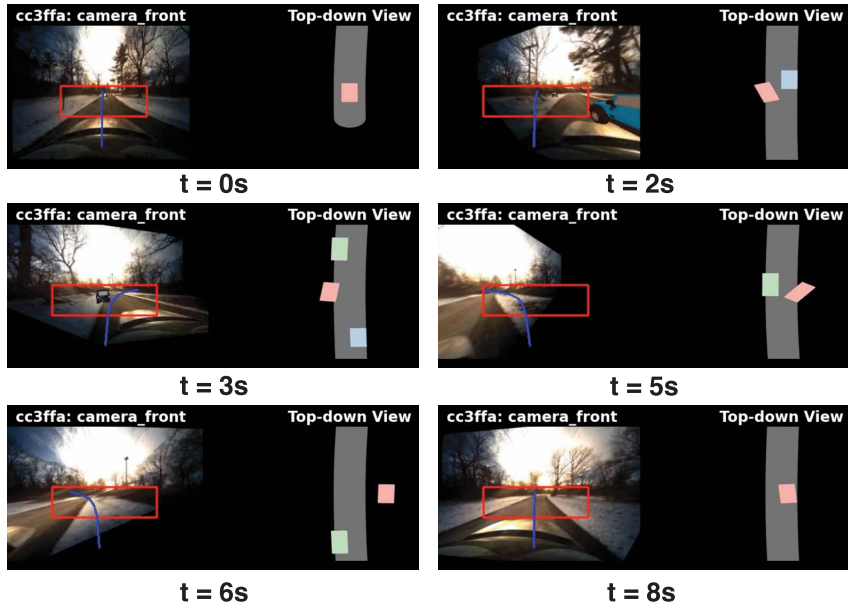


Figure 11. Qualitative visualization of closed-loop driving behaviors in the VISTA simulator using ABNet. Each snapshot corresponds to the same set of time steps as in Fig. 10 (timestamps shown above each panel). The left image shows the front-view camera observation and the right image shows the corresponding top-down view. Compared with PoSafeNet, ABNet without lane keeping constraint exhibits less consistent lane tracking.